

Water-Robust Zinc–Organic Framework with Mixed Nodes and Its Handy Mixed-Matrix Membrane for Highly Effective Luminescent Detection of Fe^{3+} , CrO_4^{2-} , and $\text{Cr}_2\text{O}_7^{2-}$ in Aqueous Solution

Bowen Qin, Xiaoying Zhang,* Jingjing Qiu, Godefroid Gahungu, Haiyan Yuan,* and Jingping Zhang*

Cite This: *Inorg. Chem.* 2021, 60, 1716–1725

Read Online

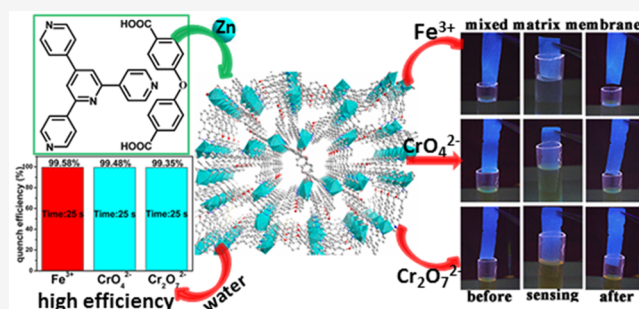
ACCESS |

Metrics & More

Article Recommendations

Supporting Information

ABSTRACT: Metal–organic frameworks (MOFs) and MOF-based composites as luminescent sensors with excellent economic practicability and handy operability have attracted much attention. Herein, we designed and fabricated a porous Zn-based MOF, $[\text{Zn}(\text{OBA})_2(\text{L}_1)\cdot 2\text{DMA}]_n$ [**1**; $\text{H}_2\text{OBA} = 4,4'$ -oxybis(benzoic acid), $\text{L}_1 = 2,4,6$ -tris(4-pyridyl)pyridine, and $\text{DMA} = N,N$ -dimethylacetamide], with mixed nodes under solvothermal conditions, and the pore size of 5.9 Å was calculated from N_2 adsorption isotherms by using a density functional theory model. The as-synthesized compound **1** is stable in different boiling organic solvents and water solutions with a wide pH range of 2–12 and exhibits intense luminescence emission at 360 nm under excitation of 290 nm. Significantly, compound **1** shows high selective detection of Fe^{3+} , CrO_4^{2-} , and $\text{Cr}_2\text{O}_7^{2-}$ in aqueous solution even under the interference of other ions. Compound **1** can quickly sense these ions in a short time and has a striking sensitivity toward Fe^{3+} with an ultralow limit of detection (LOD) of 1.06 μM . The relatively low LODs for CrO_4^{2-} and $\text{Cr}_2\text{O}_7^{2-}$ are 3.87 and 2.37 μM , respectively, compared to the reported works. Meanwhile, compound **1** can be reused to detect Fe^{3+} , CrO_4^{2-} , and $\text{Cr}_2\text{O}_7^{2-}$ six times by simple regeneration. Considering the practicability, a mixed-matrix membrane (MMM) incorporated compound **1** and poly(methyl methacrylate) has been constructed. This MMM displays quick detection of Fe^{3+} , CrO_4^{2-} , and $\text{Cr}_2\text{O}_7^{2-}$ and prompt regeneration by lifting from the analyte. This useful MMM shows a comparable LOD below 4.35 μM for these ions. This work presents a cost-effective Zn-based MOF as a functional platform for simple but useful sensing of Fe^{3+} , CrO_4^{2-} , and $\text{Cr}_2\text{O}_7^{2-}$ in aqueous solution.



1. INTRODUCTION

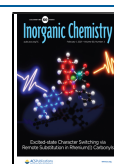
The detection of heavy-metal ions is necessary because of their toxicity and bioaccumulation in a living body.^{1–5} For instance, Fe^{3+} plays indispensable roles in the processes of hemoglobin formation, oxygen uptake, and the syntheses of DNA and RNA.⁶ Both deficiency and excess of Fe^{3+} can lead to serious biological disorders.⁷ Similarly, hexavalent chromium existing as the soluble anion $\text{CrO}_4^{2-}/\text{Cr}_2\text{O}_7^{2-}$ is highly carcinogenic and can destroy DNA and the protein and enzyme systems of the human body even at low concentration.^{8,9} Hence, the selective detection of Fe^{3+} , CrO_4^{2-} , and $\text{Cr}_2\text{O}_7^{2-}$ is urgent and has attracted increasing interest.

Luminescent metal–organic frameworks (MOFs) with novel structures and permanent channels have been widely explored for their sensing applications in ions, pH values, explosives, and antibiotics.^{10–13} However, the luminescent MOFs detecting both Fe^{3+} and chromate ions (CrO_4^{2-} and $\text{Cr}_2\text{O}_7^{2-}$) are limited.^{14–17} Meanwhile, most of the luminescence sensing on the basis of MOFs is performed in nonaqueous media because of the poor water stability of these chemosensors.^{18–21} This unsatisfactory stability also hinders the further reuse of luminescent MOFs for sensing ions.^{22–24} Therefore, it is

imperative and challenging to design and synthesize stable MOFs retaining their integrities in different pH aqueous solutions.²⁵ Up to now, several traditional detection methods such as atomic absorption spectrometry, inductively coupled plasma atomic emission spectrometry (ICP-AES), and ion-mobility spectrometry have been available for probing these ions but are time-consuming and of high cost.^{24,26} For MOF-based sensors, complex synthesis methods and expensive raw materials including organic linkers and metal sources also limit their development and application. Herein, the abundant transition metals with d^{10} configurations and the accessible combinations of carboxylic acid and nitrogen heterocyclic ligands have been proven to be very helpful to constructing cost-effective MOFs with versatility.^{22,27–29} For example, Sun and co-workers synthesized MOF membranes with improved

Received: October 29, 2020

Published: January 20, 2021



gas separation by using imidazole and 3,3',5,5'-azobenzene-tricarboxylic acid ligands.³⁰ Furthermore, the general sensing detection of MOF materials was performed in the dispersed phases of sensors, deviating from the handy operability and repeatability, which are also significant indexes for the practical sensing of luminescent MOFs. To solve this obstacle, it is feasible to design and prepare a mixed-matrix membrane (MMM) incorporating a luminescent MOF and a polymer as a test device.^{31–34} Meanwhile, most of MOFs utilize unified nodes to construct porous frameworks.^{30,35,36} In this regard, two kinds of metal nodes incorporated into a skeleton can further improve the diversity of the skeleton and optimize the structural stability.^{25,37–41}

On the basis of the above considerations, a 3D luminescent Zn-based MOF, $[\text{Zn}(\text{OBA})_2(\text{L}_1)_2 \cdot 2\text{DMA}]_n$ (**1**; $\text{H}_2\text{OBA} = 4,4'$ -oxybis(benzoic acid), $\text{L}_1 = 2,4,6$ -tris(4-pyridyl)pyridine, and $\text{DMA} = N,N$ -dimethylacetamide; CCDC 2040578), with a pore size of 5.9 Å has been assembled by employing the low-cost V-shaped H_2OBA , the rigid nitrogen heterocyclic L_1 with a large π -conjugated system, and $\text{Zn}(\text{CH}_3\text{COO})_2 \cdot 2\text{H}_2\text{O}$ under a solvothermal method. The porous compound **1** shows satisfactory chemical stability in a H_2O solution (pH = 2–12) and different boiling organic solvents and thermal stability under 300 °C in air, inspiring the experimental exploration under hard conditions. In a series of sensing tests, we found that compound **1** can selectively detect Fe^{3+} , CrO_4^{2-} , and $\text{Cr}_2\text{O}_7^{2-}$ in a short response time in aqueous solution. Moreover, these quenching detections could not be interfered with even in the presence of other cations and anions. Meanwhile, compound **1** shows low limits of detection (LODs) toward Fe^{3+} , CrO_4^{2-} , and $\text{Cr}_2\text{O}_7^{2-}$ of 1.06, 3.87, and 2.37 μM , confirming excellent sensitivity of this compound. In addition, compound **1** can be easily and quickly recovered and then reused six times, confirming the good recyclability. To further improve the potential for practical applications, we designed and prepared a MMM incorporating compound **1** and poly(methyl methacrylate) (PMMA), showing blue emission. This MMM can quickly detect Fe^{3+} , CrO_4^{2-} , and $\text{Cr}_2\text{O}_7^{2-}$ and then be regenerated by lifting from the analytical solutions, demonstrating its quick response and good selectivity. The experiments further indicate that this MMM possesses a comparable LOD below 4.35 μM for these three kinds of ions. Therefore, compound **1** is an excellent chemosensor.

2. EXPERIMENTAL SECTION

2.1. Materials and Methods. All chemicals used in this work were purchased commercially and employed without further purification. The ligand L_1 was prepared according to the previous method with some modification.⁴² The ^1H NMR spectrum was measured with a Bruker Avance Neo 500 MHz spectrometer. Powder X-ray diffraction (PXRD) was performed with a SmartLab X-ray diffractometer equipped with $\text{Cu K}\alpha$ ($\lambda = 1.54184$ Å) radiation and a graphite monochromator in the range of 5–40°. The data of thermogravimetric analysis (TGA) were collected by using a Rigaku PTC-10ATG-DTA analyzer under a N_2 atmosphere with a heating speed of 10 °C min^{-1} from room temperature to 800 °C. An Elementar Vario EL analyzer was employed to perform elemental analyses (C, H, and N). The Micromeritics ASAP 2020 M gas adsorption analyzer was used to test gas adsorption. The luminescence spectra were recorded by utilizing a FLSP920 Edinburgh fluorescence spectrometer with a slit width of 1.0 nm. A Leeman Laboratories Prodigy ICP-AES system was used to conduct ICP analyses. The UV–vis absorption spectra were recorded by

employing a MAPADA P7 double-beam UV–vis spectrophotometer with the range of 200–800 nm at room temperature.

2.2. Synthesis of Ligand L_1 . In a round-bottom flask (250 mL), a mixture of 4-pyridinecarboxaldehyde (2.14 g, 20 mmol) and 4-acetylpyridine (4.85 g, 40 mmol) was dispersed in $\text{CH}_3\text{CH}_2\text{OH}$ (100 mL). A KOH aqueous solution (2.8 g, 50 mmol, 85%) was then added, and the solution was stirred for 2 h at 0 °C. Subsequently, an ammonia solution (70 mL, 25%) was charged into this mixture. Then, the reaction mixture was heated and refluxed for 12 h. After complete reaction, the mixture was cooled at 0 °C for 1 h, and the light-purple L_1 ligand (2.98 g, 9.61 mmol, yield 48%) was collected by filtration and washed with ice-cold $\text{CH}_3\text{CH}_2\text{OH}$ (100 mL). ^1H NMR (CDCl_3 , 500 MHz): δ 8.84 (s, 4H), 8.82 (d, 2H), 8.10 (d, 4H), 8.06 (s, 2H), 7.66 (d, 2H).

2.3. Synthesis of $[\text{Zn}(\text{OBA})_2(\text{L}_1)_2 \cdot 2\text{DMA}]_n$ (1**).** A mixture of H_2OBA (0.065 g, 0.25 mmol), L_1 ligand (0.045 g, 0.15 mmol), and $\text{Zn}(\text{CH}_3\text{COO})_2 \cdot 2\text{H}_2\text{O}$ (0.11 g, 0.5 mmol) in 8 mL of DMA was placed in a 23 mL Teflon-lined stainless steel autoclave. The mixture was heated in a 120 °C oven for 72 h (Scheme S1). After cooling to room temperature, the colorless crystals of compound **1** were harvested (yield: 85% based on H_2OBA). Elem anal. Calcd for $\text{C}_{56}\text{H}_{48}\text{N}_6\text{O}_{12}\text{Zn}_2$ (1127.74): C, 59.64; H, 4.29; N, 7.45. Found: C, 59.58; H, 4.32; N, 7.43.

2.4. X-ray Structure Determination. A Bruker D8 VENTURE diffractometer equipped with graphite-monochromated $\text{Mo K}\alpha$ radiation ($\lambda = 0.71073$ Å) was employed to collect diffraction data of compound **1** under the ϕ and ω scan techniques. The crystal structure was solved by direct methods, and all of the non-hydrogen atoms were refined anisotropically on F^2 by full-matrix least squares with the SHELXL package.⁴³ Crystallographic data and structure refinement are exhibited in Table S1. We also listed the selected bond lengths and angles in Table S2. Full crystallographic data are stored in CCDC 2040578.

2.5. Activation of Compound **1.** The fresh synthesized compound **1** was washed with DMA and soaked for 3 days in CH_3OH , during which the solvent was poured out and fresh solvent was charged every 12 h. Then the solid samples were dried in a vacuum oven at 150 °C. The structure of activated compound **1** was maintained, as confirmed by the PXRD pattern (Figure S1).

2.6. Luminescence Sensing Experiments. All sensing experiments were performed at ambient temperature. A total of 75 mg of ground compound **1** was added to a 250 mL volumetric flask, and H_2O was charged to form a suspension (0.3 mg mL^{-1}) by ultrasonication for 10 min. For ion-sensing experiments, 9 mL of an aqueous suspension of compound **1** and 1 mL of the corresponding $\text{M}(\text{NO}_3)_x$ ($\text{M} = \text{Zn}^{2+}$, Co^{2+} , Cd^{2+} , Mg^{2+} , K^+ , Ni^{2+} , Mn^{2+} , Na^+ , Fe^{3+} , Cr^{3+} , Pb^{2+} , Cu^{2+} , and Al^{3+}) or NaX ($\text{X} = \text{PO}_4^{3-}$, CO_3^{2-} , NO_3^- , ClO_4^- , Cl^- , Br^- , SO_4^{2-} , NO_2^- , CrO_4^{2-} , and $\text{Cr}_2\text{O}_7^{2-}$) aqueous solution (10 mM) were well mixed. The antijamming experiments were carried out by mixing 9 mL of an aqueous suspension of compound **1**, 0.5 mL of a Fe^{3+} , CrO_4^{2-} , and $\text{Cr}_2\text{O}_7^{2-}$ aqueous solution (20 mM), and 0.5 mL of different interfering ion aqueous solutions (20 mM). The luminescence titration experiments of cations and anions were performed by adding step by step a Fe^{3+} , CrO_4^{2-} , and $\text{Cr}_2\text{O}_7^{2-}$ aqueous solution (10 mM) to 10 mL of a compound **1** suspension, respectively.

2.7. Preparation of MMMs Incorporating Compound **1.** Compound **1** (50 mg) with adequate grinding was added to a PMMA/chloroform solution (50 mL, 20 mg mL^{-1}), and then the dispersed suspensions were ultrasonicated for 0.5 h. The luminescent MMMs with a mass loading of 5% were formed by pouring and tiling the above mixed slurry on culture ware, followed by heating in an oven at 40 °C overnight. The free-standing luminescent MMMs with uniform size (1.0 cm \times 3.6 cm) were obtained by peeling from culture ware and shearing.

3. RESULTS AND DISCUSSION

3.1. Crystal Structure. Single-crystal X-ray diffraction analysis revealed that compound **1** crystallized in a monoclinic

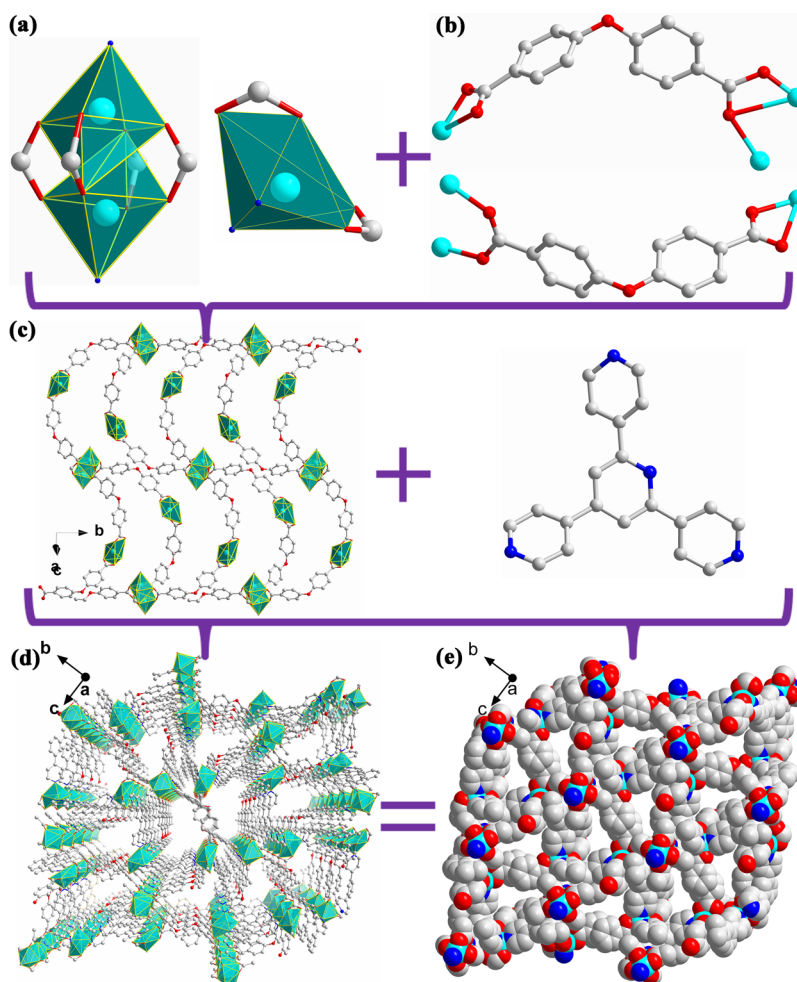


Figure 1. Crystal structure of compound **1**: (a) coordination environment of Zn^{2+} in compound **1**; (b) coordination nodes of the OBA^{2-} ligand; (c) 2D layer of compound **1** and L_1 ligand; (d) 3D structure viewed along the a axis; (e) space-filling diagram of compound **1** viewed along the a axis. Color code: C, light gray; O, red; N, blue; Zn, turquoise.

crystal system with space group $P2_1/c$. As presented in Figure S2, the asymmetric unit of compound **1** consists of two crystallographically independent Zn^{2+} , two OBA^{2-} ligands, and one independent L_1 ligand. Zn1 is in a $[\text{ZnO}_4\text{N}_2]$ distorted octahedral geometry defined by four oxygen atoms (O1, O2, O7A, and O8A) from two OBA^{2-} ligands with Zn1–O bond lengths in the range of 1.938(6)–2.702(6) Å and two nitrogen atoms from two L_1 ligands with Zn1–N bond distances falling in 2.033(6)–2.107(6) Å (Figure 1a). The 6-connected Zn2 is coordinated by five carboxyl oxygen atoms (O3, O5, O4D, O5D, and O6D) from four different OBA^{2-} ligands and one nitrogen atom (N2C) from one L_1 ligand, resulting in an irregular octahedral coordination geometry. The Zn2–O and Zn2–N distances fall into the range of 1.779(14)–2.773(6) Å and 2.009(6) Å, respectively. All Zn–O and Zn–N bond distances of Zn1 and Zn2 match well with those reported previously.^{44,45} It is worth noting that one independent Zn1 atom forms a mononuclear $[\text{Zn}(\text{COO})_2\text{N}_2]$ node and two adjacent Zn2 atoms construct a binuclear $[\text{Zn}_2(\text{COO})_4\text{N}_2]$ node (Figure 1a). The $[\text{Zn}(\text{COO})_2\text{N}_2]$ and $[\text{Zn}_2(\text{COO})_4\text{N}_2]$ nodes are connected by OBA^{2-} ligands adopting $\mu_3:\eta^1:\eta^1:\eta^1:\eta^2$ and $\mu_3:\eta^1:\eta^1:\eta^1:\eta^1$ coordination nodes (Figure 1b), forming a fish-scale 2D layer with a window size of $18.75 \times 8.27 \text{ \AA}^2$ taking the van der Waals radius into account (Figure 1c). As shown in Figure 1d, the novel 2D layers of compound **1** are

further linked by L_1 ligands, finally constructing a 3D porous framework. From the view of topology,⁴⁶ the OBA^{2-} ligand, L_1 ligand, mononuclear Zn unit, and binuclear Zn unit can be considered to be 2-, 3-, 4-, and 6-connected nodes, respectively (Figure S3). In particular, the OBA^{2-} ligands exhibit two kinds of 2-connected models. Thus, compound **1** can be described as a $2,2,3,4,6$ -connected net with a short Schläfli symbol of $\{4 \cdot 8 \times 10\}_2\{4 \cdot 8 \cdot 12^4\}_2\{4^2 \cdot 8^2 \cdot 10^2 \cdot 12^7 \cdot 14 \cdot 16\}\{4\}_2\{8\}_2$ (Figure S3). The scalene 1D channel can be seen along the a axis (Figure 1e), and the total solvent-accessible volume calculated by the PLATON software is 31.7%.⁴⁷

3.2. Framework Stability. Prior to performance analysis, the PXRD experiments were conducted for confirming the phase purity of compound **1**. A comparison of the peaks shows good consistency between the experimental and simulated PXRD patterns (Figure S4), confirming the excellent phase purity of the polycrystalline sample. In order to further investigate the chemical stability of compound **1**, 25 mg of the as-synthesized sample was immersed in various acid/base aqueous solutions with pH values ranging of 2–12 and different boiling solvents (ethyl acetate, CH_3OH , CHCl_3 , CH_2Cl_2 , n -hexane, isopropyl alcohol, N -methyl-2-pyrrolidone, N,N -diethylformamide, acetone, $\text{CH}_3\text{CH}_2\text{OH}$, CH_3CN , DMA, N,N -dimethylformamide, and H_2O) for 12 h, respectively. The corresponding PXRD patterns of compound **1** after treated are

in agreement with the peak positions of the as-synthesized sample, indicating that the structure of compound **1** is still intact in these solutions (Figure 2a,b). According to the hard–

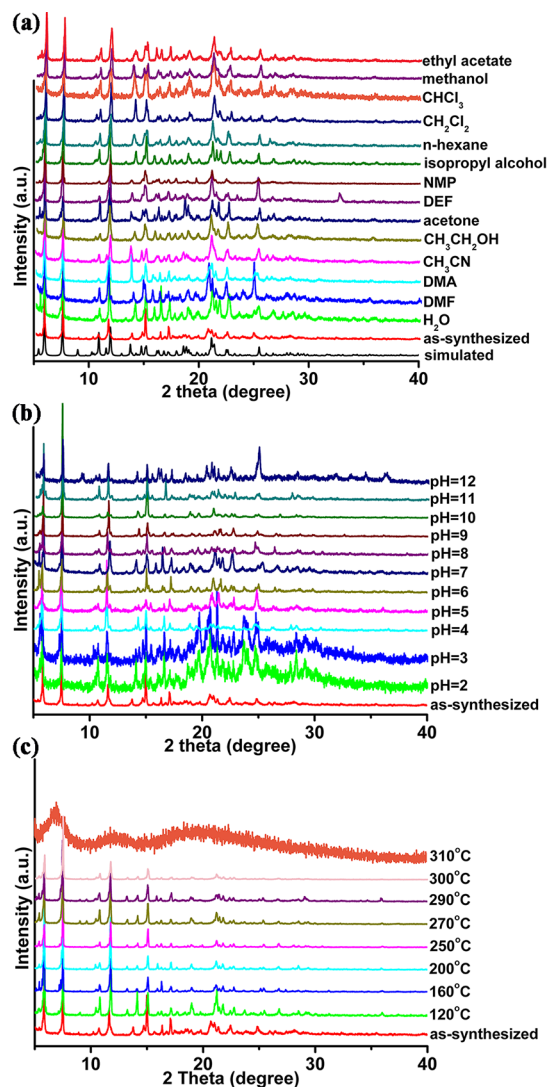


Figure 2. Stability exploration of compound **1**: (a) PXRD patterns of compound **1** after being immersed in different boiling solvents for 24 h; (b) PXRD patterns of compound **1** after being soaked in H₂O with different pH values (2–12) for 24 h; (c) PXRD patterns of compound **1** after being heated at different temperatures in air.

soft acid–base theory, the Zn²⁺ ions as soft acids tend to bind with N-containing linkers as soft bases to construct stable structures.²⁵ Zn and N in compound **1** form a strong bonding interaction, which can reduce the damage of coordination bonds in H₂O. The hydrophobic benzene rings and saturated coordination nodes in compound **1** can effectively protect the coordination bonds from the attack by H₂O and enhance the framework stability in aqueous solution.⁴⁵ As reported in the previous literature, the mixed ligands combining mixed-donor linkers (N and O donors) can also enhance the stability of MOFs in H₂O.^{49–52} To further explore the thermal stability of compound **1**, TGA measurement was carried out from room temperature to 800 °C under a N₂ atmosphere. As shown in Figure S5, a weight loss of about 13.22% can be observed at 90–265 °C (calcd 15.3%), corresponding to the escape of two

free DMA molecules. Upon further heating, no weight loss can be found up to 325 °C because there is a platform in the range of 265–325 °C and the framework begins to collapse at higher temperatures. Meanwhile, we heated the fresh compound **1** at different temperatures in air, and the PXRD patterns of compound **1** heated to 300 °C match closely with that of the fresh sample (Figure 2c).

The above results indicate that compound **1** possesses excellent chemical and thermal stabilities because it can retain its integrity in H₂O (pH = 2–12), in different boiling solvents, and at high temperature (300 °C) in air.

3.3. Gas Adsorption. The permanent porosity of activated compound **1** was tested by N₂ adsorption–desorption isotherms at 77 K. As shown in Figure 3a, compound **1**

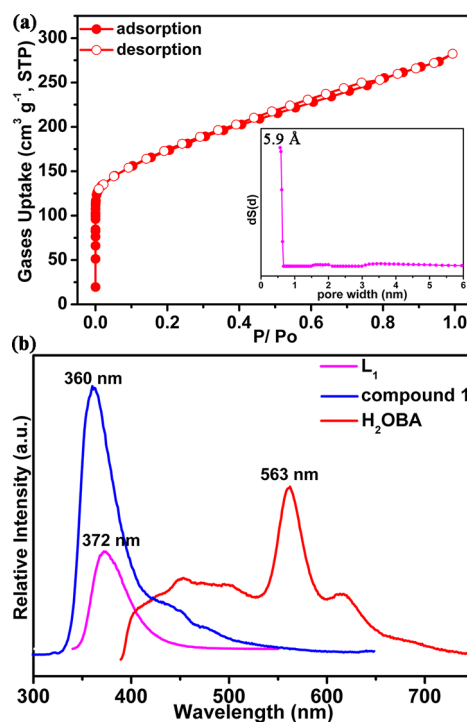


Figure 3. (a) N₂ adsorption isotherm of compound **1** at 77 K. (b) Emission spectra of H₂OBA ligand (λ_{ex} = 346 nm), L₁ ligand (λ_{ex} = 290 nm), and compound **1** (λ_{ex} = 290 nm).

exhibits type I adsorption isotherms, which is classic for microporous materials. The adsorption amount of N₂ at 1 atm reached 282 cm³ g⁻¹. The Brunauer–Emmett–Teller and Langmuir surface areas are 573 and 882 m² g⁻¹, respectively. Meanwhile, the pore size is 5.9 Å, calculated by using the density functional theory (DFT) model, further confirming its microporosity. Furthermore, the H₂ adsorption isotherms for compound **1** were measured at 77 K (Figure S6). The H₂ uptake of compound **1** reaches a maximum of 97.3 cm³ g⁻¹ at 1 atm. This adsorption amount is higher than those of some reported porous materials,^{53–55} indicating its potential application for H₂ adsorption and storage.

3.4. Luminescence Sensing of Compound 1. Because the aromatic ligands and d¹⁰ metal centers can be used to construct promising MOFs with potential luminescence, we explored the luminescent properties of the free ligands and compound **1**. As shown in Figures 3b and S7, the emission spectra of the H₂OBA and L₁ ligands exhibit moderate intensity with emission maxima at 563 and 372 nm (λ_{ex} = 346

and 290 nm), respectively. These emissions may be assigned to the intraligand $\pi \rightarrow \pi^*$ and/or $n \rightarrow \pi^*$ charge transitions. Meanwhile, compound **1** exhibits an enhanced emission peak at 360 nm under excitation at 290 nm, indicating that the luminescence emission of this Zn-based MOF originates from the L_1 ligand.⁵⁶ Compared to the L_1 ligand, the emission of compound **1** is blue-shifted by 12 nm and distinctly enhanced, which may be caused by the constrained coordination of Zn^{2+} with the organic ligands in the stable framework. The emission spectra of compound **1** under different excitation wavelengths were also measured, which do not show emission peaks similar to the 563 nm peak of H_2OBA (Figure S8). Furthermore, the wavelength of the maximum emission exhibits obvious shifts when compound **1** is dispersed in various organic solvents such as CH_3OH , CH_3CH_2OH , ethyl acetate, isopropyl alcohol, *N*-methyl-2-pyrrolidone, CH_3CN (Figure S9). This phenomenon confirms that compound **1** could be employed to identify different organic solvents through the wavelength shifts.⁵⁷

Inspired by the excellent water stability, strong luminescence intensity, and aromatic pyridine rings of compound **1**, the luminescence detection toward metal cations was investigated. Thus, a suspension of compound **1** was fully mixed with aqueous solutions of $M(NO_3)_x$ ($M = Zn^{2+}$, Co^{2+} , Cd^{2+} , Mg^{2+} , K^+ , Ni^{2+} , Mn^{2+} , Na^+ , Fe^{3+} , Cr^{3+} , Pb^{2+} , Cu^{2+} , and Al^{3+}), respectively. The emission spectra of suspensions incorporating metal ions with an ion concentration of 1 mM were recorded (Figure S10a). As illustrated in Figure 4a, the

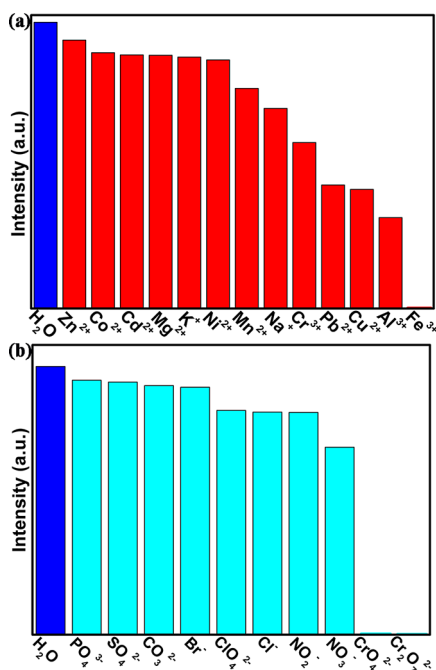


Figure 4. Luminescence intensities of compound **1** dispersed in aqueous solutions of different (a) cations and (b) anions (1 mM) under excitation at 290 nm.

luminescence intensity of compound **1** is influenced by the metal ions. In particular, the luminescence of compound **1** is almost completely quenching toward Fe^{3+} with a quenching efficiency of 99.96%, while the quenching percentages of other ions are negligible or moderate. This reveals that compound **1** can selectively detect Fe^{3+} over other explored cations. More importantly, Fe^{3+} leads to the dominant luminescence quenching of compound **1** even in the presence of other

disturbing cations, indicating that compound **1** possesses excellent selectivity for Fe^{3+} (Figure S11).

Meanwhile, we also explored the selective recognition of compound **1** toward different anions (NaX , where $X = PO_4^{3-}$, CO_3^{2-} , NO_3^- , ClO_4^- , Cl^- , Br^- , SO_4^{2-} , NO_2^- , CrO_4^{2-} , $Cr_2O_7^{2-}$). Similar to the cation-sensing experiments, the luminescence intensities of aqueous suspensions containing compound **1** and various anions (1 mM) were measured (Figure S10b). As shown in Figure 4b, most tremendous quenching effects are observed in the presence of CrO_4^{2-} and $Cr_2O_7^{2-}$, but other ions make compound **1** have negligible quenching. The effective quenching efficiencies of CrO_4^{2-} and $Cr_2O_7^{2-}$ are 99.84% and 99.88%, respectively. Selective quenching of compound **1** to chromate ions was explored by interference tests. The other anions do not obstruct the significant quenching of compound **1** with the addition of CrO_4^{2-} and $Cr_2O_7^{2-}$ (Figures S12 and S13), suggesting the perfectly selective sensing and antiinterference capability of compound **1** for chromate ions in aqueous solution.

Besides the satisfactory selectivity, the performance indexes with short response time, excellent sensitivity, low LOD, and well recyclability are also crucial to compound **1** as a feasible chemosensor. To explore the response time of the three kinds of ions, we charged separately 1 mL of a Fe^{3+} , CrO_4^{2-} , or $Cr_2O_7^{2-}$ aqueous solution (10 mM) to glass sample bottle with 9 mL of an aqueous dispersion of compound **1** and quickly shook to well mix. Subsequently, we recorded the corresponding luminescence spectra. As shown in Figure 5a, the luminescence of compound **1** quenches rapidly and the quenching efficiency is almost 100% in 25 s after the addition of the corresponding ions (Fe^{3+} , 99.58%; CrO_4^{2-} , 99.48%; $Cr_2O_7^{2-}$, 99.35%). This striking result indicates the fast response rate and short response time of compound **1** for Fe^{3+} , CrO_4^{2-} , and $Cr_2O_7^{2-}$. Simultaneously, three kinds of ion aqueous solutions (10 mM) were titrated gradually into a suspension of compound **1** to study the sensitivity of this chemosensor. In the antiinterference and titration experiments, the maximum emission wavelength deviated in the blank experiments, which may be due to insufficient grinding of the MOF material and the short ultrasonic treatment time, resulting in the uneven particle size of compound **1** in H_2O . Following an increase of the Fe^{3+} concentration, the luminescence intensity of compound **1** gradually weakened (Figure S14a). Similar results were also observed in the related experiments of CrO_4^{2-} and $Cr_2O_7^{2-}$ (Figure S14). To further evaluate the sensitivity of compound **1**, the Stern–Volmer (S–V) equation ($I_0/I = 1 + K_{SV} [M]$, where K_{SV} is the quenching constant, $[M]$ is the ion concentration, I_0 and I are the luminescence intensities of the suspension before and after the addition of ion aqueous solutions) was employed to analyze the luminescence quenching efficiency. As shown in Figure 5, the S–V curves for Fe^{3+} , CrO_4^{2-} , and $Cr_2O_7^{2-}$ show a good linear correlation ($R^2 = 0.99$, 0.97, and 0.99) in the concentration ranges of 0–0.1, 0–0.183, and 0–0.21 mM, respectively. The calculated K_{SV} of Fe^{3+} is $42210.27 M^{-1}$, which is much higher than those in some reported works.^{14,58,59} Furthermore, the LOD of compound **1** toward Fe^{3+} is calculated by using the equation of $LOD = 3\sigma/\text{slope}$ (σ = standard deviation) with a low LOD of $1.06 \mu M$. Meanwhile, the K_{SV} and LOD of compound **1** toward $CrO_4^{2-}/Cr_2O_7^{2-}$ are $11605.28 M^{-1}$ and $3.87 \mu M$ and $18972.72 M^{-1}$ and $2.37 \mu M$, respectively. The LOD values of this compound for Fe^{3+} , CrO_4^{2-} , and $Cr_2O_7^{2-}$ are comparable to those reported

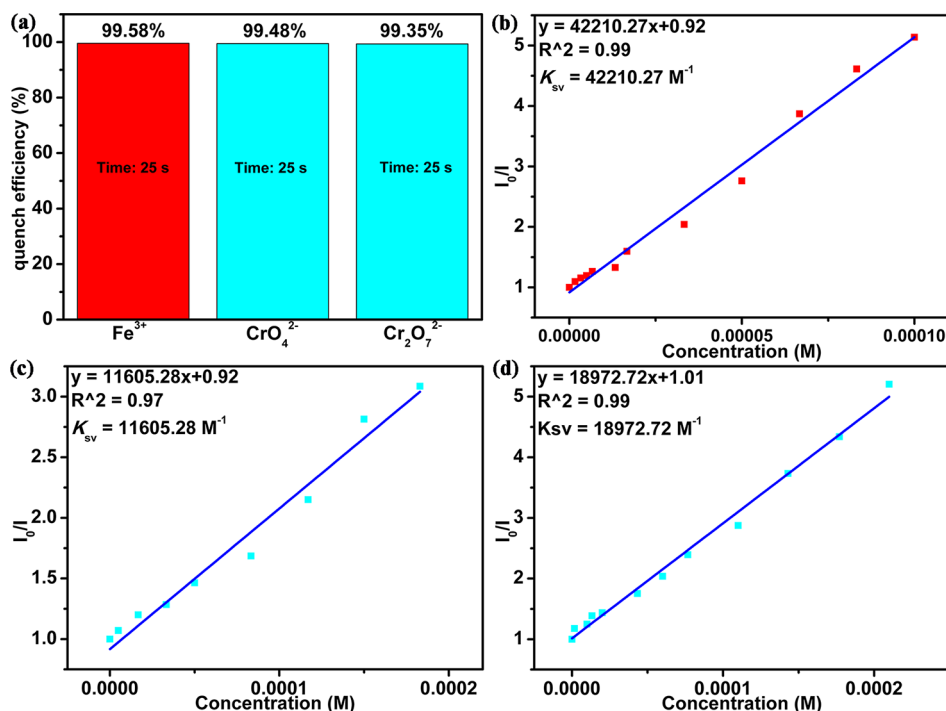


Figure 5. (a) Quenching efficiencies of compound **1** for Fe³⁺, CrO₄²⁻, and Cr₂O₇²⁻ in 25 s. S–V plots of I₀/I versus concentrations of Fe³⁺ (b), CrO₄²⁻ (c), and Cr₂O₇²⁻ (d), respectively.

previously, further confirming the potential application of compound **1** as a chemosensor toward these ions (Tables S3–S5).^{14,58–68}

In order to further explore the practicability of this chemosensor, the recycling experiments were carried out as follows: compound **1** after grinding was placed in a H₂O solution of Fe³⁺, CrO₄²⁻, and Cr₂O₇²⁻, respectively, and the mixture was sonicated for several minutes. Then, we tested the corresponding luminescence spectra, and the sample in suspension solutions was washed with deionized water and centrifuged several times. Subsequently, the recovered sample was confirmed by luminescence spectra (Figure S15). We repeated the above experiments several times. As shown in Figure 6, compound **1** can be simply and quickly regenerated and reused to detect Fe³⁺, CrO₄²⁻, and Cr₂O₇²⁻ six times, suggesting excellent recyclability. It is noted that the luminescence intensity of compound **1** was reduced by half after six cycles, indicating the strong interaction between Fe³⁺ and the framework of compound **1**. After six cycles, the Fe³⁺ content of compound **1** is 0.64 wt %, which was measured by ICP analysis.

The above experiments demonstrate that luminescent compound **1** has excellent selectivity, short response time, high sensitivity, low LOD, and well recyclability toward Fe³⁺, CrO₄²⁻, and Cr₂O₇²⁻. Therefore, the mechanism investigation is very necessary to further design a useful luminescent chemosensor. First, the PXRD patterns of the samples were recorded after immersion into a 1 mM aqueous solution of Fe³⁺, CrO₄²⁻, and Cr₂O₇²⁻ for 24 h (Figure S16). There is no change in the peaks compared to the as-synthesized compound **1**, confirming that the structure is maintained even during the sensing process and the luminescence quenching should not be due to the structural collapse of this compound. To further confirm the possible quenching mechanism of compound **1** toward these ions, UV–vis absorption spectra of the aqueous

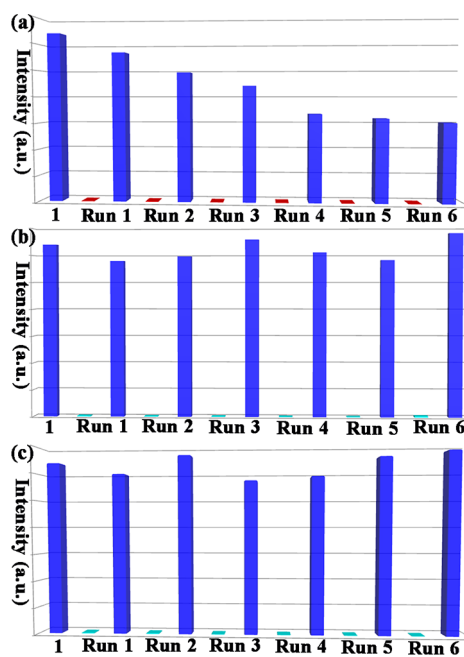


Figure 6. Six cycle experiments of compound **1** for sensing Fe³⁺ (a), CrO₄²⁻ (b), and Cr₂O₇²⁻ (c).

solutions of anions and cations (1 mM) were recorded and analyzed. It is apparent that Fe³⁺ shows an absorption band from 200 to 450 nm, which covers the excitation spectrum of compound **1** (270–330 nm). However, no overlap can be observed between the UV–vis absorption bands of other cations and the excitation spectrum of this luminescence sensor (Figure S17a).^{59,63} Therefore, it is very likely that Fe³⁺ can compete with this MOF for absorbing the excitation light. Therefore, the competitive absorption between Fe³⁺ and compound **1** cut down the excitation efficiency, resulting in

emission quenching. Meanwhile, the broad absorption bands of CrO_4^{2-} and $\text{Cr}_2\text{O}_7^{2-}$ from 320 to 480 nm nearly cover the emission spectrum of compound **1** (320–500 nm), which does not overlap with the UV–vis absorption peaks of other anions (Figure S17b). Therefore, resonance energy transfer from compound **1** (donor) to the CrO_4^{2-} and $\text{Cr}_2\text{O}_7^{2-}$ ions (acceptors) might occur and lead to luminescence quenching.^{58,65} In addition, compound **1** can encapsulate Al^{3+} , Cu^{2+} , and Pb^{2+} because it has microporous channels. As shown in Table S6, the results of ICP-ACS also confirmed the successful introduction of these ions into compound **1**. The introduction of Al^{3+} , Cu^{2+} , and Pb^{2+} may consume energy through the collision interaction between ions and the framework and further decrease the energy-transfer efficiency within the framework, leading to the reduction of luminescence of compound **1**.^{69,70} The size and electron configuration of the three ions are different, so they have different effects on fluorescence attenuation.^{71,72}

3.5. Luminescent MMMs of Compound 1. Inspired by the excellent stability and sensing performance in a H_2O solution, the luminescent MMMs were designed and prepared to improve the convenience of operation and expand the practical application of compound **1**. As shown in Figure 7a, the uniform membrane was prepared through the complete mixing of compound **1** and PMMA in CH_2Cl_2 . The PXRD spectrum of this MMM contains the peaks of compound **1**, indicating that this compound retains its structural integrity in the process of membrane preparation (Figure 7b). Meanwhile,

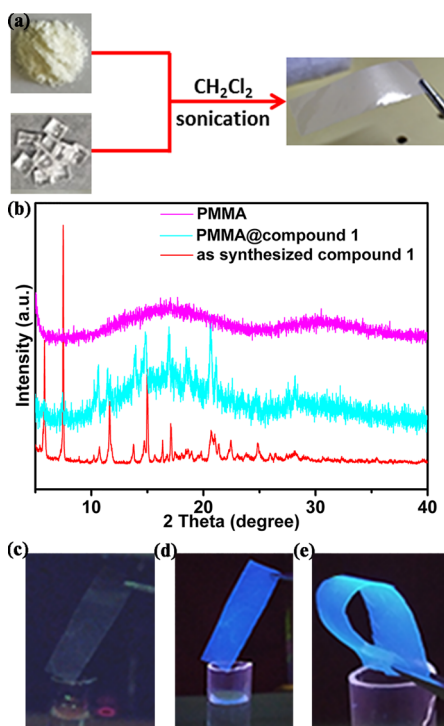


Figure 7. (a) Schematic illustration for the preparation process of MMM incorporating compound **1** (the powder is compound **1**; the transparent blocks are PMMA). (b) PXRD patterns of PMMA, MMM, and the as-synthesized compound **1**. Photographs of luminescent MMM incorporating compound **1** in a dark room (c) and upon UV-light irradiation of 254 nm (d). (e) Photographs demonstrating that large-area MMM is resilient to mechanical stress and can be easily handled.

the MMM cannot emit fluorescence in a dark room (Figure 7c) but shows strong blue emission under irradiation of a laboratory UV lamp (254 nm). Under the same conditions, the pure membrane PMMA only exhibits weak emission (Figure S18), confirming that the emission source is compound **1**. The uniform brightness also confirms the homogeneous distribution of compound **1** in this MMM (Figure 7d). Besides, the MMMs show good toughness because it can be bent (Figure 7e). The above properties indicate the great potential of this test device for luminescence sensing application. When MMM was gradually immersed in the Fe^{3+} , CrO_4^{2-} , and $\text{Cr}_2\text{O}_7^{2-}$ aqueous solution, respectively, the strong blue luminescence of MMM promptly disappeared with irradiation of a laboratory UV lamp at 254 nm. Meanwhile, the fluorescence emission of MMM has no obvious change in other ionic aqueous solutions (Figures S19 and S20). Remarkably, blue luminescence can be immediately regenerated by simply removing MMM from the aqueous solution of Fe^{3+} , CrO_4^{2-} , and $\text{Cr}_2\text{O}_7^{2-}$ (Figure 8).

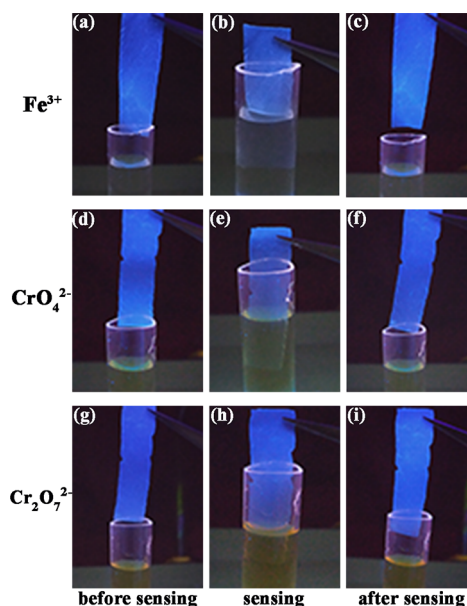


Figure 8. Photographs exhibiting the change of luminescence emission of luminescent MMM before, during, and after sensing of Fe^{3+} (a–c), CrO_4^{2-} (d–f), and $\text{Cr}_2\text{O}_7^{2-}$ (g–i) under UV-lamp irradiation ($\lambda_{\text{ex}} = 254 \text{ nm}$).

These dramatic results suggest that this MMM can quickly detect these ions and then be easily recovered, making this material have good practicability. To further explore the sensitivity of MMM for these three kinds of ions, we quantified the quenching efficiency including K_{SV} and LOD by the titration experiments (Figure S21). As illustrated in Figure S22, the S–V plots satisfy a linear relationship between the luminescence intensity and concentration of Fe^{3+} , CrO_4^{2-} , and $\text{Cr}_2\text{O}_7^{2-}$ in the range of 0–120 μM , with calculated K_{SV} values being 10330, 13000, and 12600 M^{-1} , respectively. Moreover, the LODs are estimated to be 4.35 μM for Fe^{3+} , 3.46 μM for CrO_4^{2-} , and 3.57 μM for $\text{Cr}_2\text{O}_7^{2-}$, revealing a quenching effect comparable to that of the reported luminescent MMMs. The structure of compound **1** in MMM is intact after sensing (Figure S23). These novel results suggest that this MMM can selectively detect Fe^{3+} , CrO_4^{2-} , and $\text{Cr}_2\text{O}_7^{2-}$ with short detection time and low LOD and meet the

high requirements of practical detection and fast recovery for these targeted ions.

4. CONCLUSIONS

In summary, a water-robust Zn-based MOF (**1**) with mixed nodes has been designed and synthesized by using H₂OBA ligand, L₁ ligand, and Zn(CH₃COO)₂·2H₂O under a solvothermal method. This porous compound **1** with a pore size of 5.9 Å is highly stable in different boiling organic solvents and H₂O solution with different pH values (2–12) and has strong luminescence emission. Meanwhile, compound **1** can selectively and sensitively detect Fe³⁺, CrO₄²⁻, and Cr₂O₇²⁻ with a short response time even in the presence of other interfering ions. Obviously, compound **1** can be reused six times for the detection of these ions and has a low LOD of 1.06 μM toward Fe³⁺, which is much lower than those of the reported works. The LODs for CrO₄²⁻ and Cr₂O₇²⁻ are 3.87 and 2.37 μM, which are comparable to those of the reported works. Interestingly, the luminescent MMMs, which are designed and prepared by integrating the advantages of porous MOFs and polymers, show outstanding performance with quick response, good selectivity, and excellent sensitivity. This work exhibiting an accessible luminescent MOF and a useful MOF-based MMM with excellent sensing capability to Fe³⁺, CrO₄²⁻, and Cr₂O₇²⁻ in H₂O provides valuable guidance for water-quality detection.

■ ASSOCIATED CONTENT

Supporting Information

The Supporting Information is available free of charge at <https://pubs.acs.org/doi/10.1021/acs.inorgchem.0c03214>.

Tables of crystallographic data and selected bond lengths and angles for compound **1**, PXRD pattern of compound **1** under different conditions, TGA for compound **1**, and luminescent spectra of compound **1** treated with different conditions (PDF)

Accession Codes

CCDC 2040578 contains the supplementary crystallographic data for this paper. These data can be obtained free of charge via www.ccdc.cam.ac.uk/data_request/cif, or by emailing data_request@ccdc.cam.ac.uk, or by contacting The Cambridge Crystallographic Data Centre, 12 Union Road, Cambridge CB2 1EZ, UK; fax: +44 1223 336033.

■ AUTHOR INFORMATION

Corresponding Authors

Xiaoying Zhang – Advanced Energy Materials Research Center, Faculty of Chemistry, Northeast Normal University, Changchun 130024, P. R. China; Email: zhangxy218@nenu.edu.cn

Haiyan Yuan – Advanced Energy Materials Research Center, Faculty of Chemistry, Northeast Normal University, Changchun 130024, P. R. China; Email: yuanhy034@nenu.edu.cn

Jingping Zhang – Advanced Energy Materials Research Center, Faculty of Chemistry, Northeast Normal University, Changchun 130024, P. R. China; orcid.org/0000-0001-8004-3673; Email: zhangjp162@nenu.edu.cn

Authors

Bowen Qin – Advanced Energy Materials Research Center, Faculty of Chemistry, Northeast Normal University, Changchun 130024, P. R. China

Jingjing Qiu – Advanced Energy Materials Research Center, Faculty of Chemistry, Northeast Normal University, Changchun 130024, P. R. China

Godefroid Gahungu – Department of Chemistry, University of Burundi, Bujumbura, Burundi

Complete contact information is available at: <https://pubs.acs.org/doi/10.1021/acs.inorgchem.0c03214>

Notes

The authors declare no competing financial interest.

■ ACKNOWLEDGMENTS

This work was supported by the National Natural Science Foundation of China (Grants 21873018 and 21573036), Foundation of the Education Department of Jilin Province (Grant 111099108), Fundamental Research Funds for the Central Universities (Grant 2412019QD006), Open Funds of the State Key Laboratory of Rare Earth Resource Utilization (Grant RERU2019020), and Jilin Provincial Research Center of Advanced Energy Materials (Northeast Normal University).

■ REFERENCES

- (1) Carter, K. P.; Young, A. M.; Palmer, A. E. Fluorescent sensors for measuring metal ions in living systems. *Chem. Rev.* **2014**, *114*, 4564–4601.
- (2) Raza, W.; Kukkar, D.; Saulat, H.; Raza, N.; Azam, M.; Mehmood, A.; Kim, K.-H. Metal-organic frameworks as an emerging tool for sensing various targets in aqueous and biological media. *TrAC, Trends Anal. Chem.* **2019**, *120*, 115654.
- (3) He, J.; Xu, J.; Yin, J.; Li, N.; Bu, X.-H. Recent advances in luminescent metal-organic frameworks for chemical sensors. *Sci. China Mater.* **2019**, *62*, 1655–1678.
- (4) Wang, P. L.; Xie, L. H.; Joseph, E. A.; Li, J. R.; Su, X. O.; Zhou, H. C. Metal-Organic Frameworks for Food Safety. *Chem. Rev.* **2019**, *119*, 10638–10690.
- (5) Dalmieda, J.; Kruse, P. Metal Cation Detection in Drinking Water. *Sensors* **2019**, *19*, 5134.
- (6) Que, E. L.; Domaille, D. W.; Chang, C. J. Metals in Neurobiology: Probing Their Chemistry and Biology with Molecular Imaging. *Chem. Rev.* **2008**, *108*, 1517–1549.
- (7) Cao, L. H.; Shi, F.; Zhang, W. M.; Zang, S. Q.; Mak, T. C. Selective Sensing of Fe³⁺ and Al³⁺ Ions and Detection of 2,4,6-Trinitrophenol by a Water-Stable Terbium-Based Metal-Organic Framework. *Chem. - Eur. J.* **2015**, *21*, 15705–15712.
- (8) Lustig, W. P.; Mukherjee, S.; Rudd, N. D.; Desai, A. V.; Li, J.; Ghosh, S. K. Metal-organic frameworks: functional luminescent and photonic materials for sensing applications. *Chem. Soc. Rev.* **2017**, *46*, 3242–3285.
- (9) Liu, W.; Wang, Y.; Bai, Z.; Li, Y.; Wang, Y.; Chen, L.; Xu, L.; Diwu, J.; Chai, Z.; Wang, S. Hydrolytically Stable Luminescent Cationic Metal Organic Framework for Highly Sensitive and Selective Sensing of Chromate Anions in Natural Water Systems. *ACS Appl. Mater. Interfaces* **2017**, *9*, 16448–16457.
- (10) Cui, Y.; Yue, Y.; Qian, G.; Chen, B. Luminescent functional metal-organic frameworks. *Chem. Rev.* **2012**, *112*, 1126–1162.
- (11) Kreno, L. E.; Leong, K.; Farha, O. K.; Allendorf, M.; Van Duyne, R. P.; Hupp, J. T. Metal-Organic Framework Materials as Chemical Sensors. *Chem. Rev.* **2012**, *112*, 1105–1125.
- (12) Yi, F. Y.; Chen, D.; Wu, M. K.; Han, L.; Jiang, H. L. Chemical Sensors Based on Metal-Organic Frameworks. *ChemPlusChem* **2016**, *81*, 675–690.

- (13) Jiang, H. L.; Feng, D.; Wang, K.; Gu, Z. Y.; Wei, Z.; Chen, Y. P.; Zhou, H. C. An exceptionally stable, porphyrinic Zr metal-organic framework exhibiting pH-dependent fluorescence. *J. Am. Chem. Soc.* **2013**, *135*, 13934–13938.
- (14) Chen, M.; Xu, W.-M.; Tian, J.-Y.; Cui, H.; Zhang, J.-X.; Liu, C.-S.; Du, M. A terbium(III) lanthanide-organic framework as a platform for a recyclable multi-responsive luminescent sensor. *J. Mater. Chem. C* **2017**, *5*, 2015–2021.
- (15) Li, X. S.; An, J. D.; Zhang, H. M.; Liu, J. J.; Li, Y.; Du, G. X.; Wu, X. X.; Fei, L.; Lacoste, J. D.; Cai, Z.; Liu, Y. Y.; Huo, J. Z.; Ding, B. Cluster-based Ca^{II}, Mg^{II} and Cd^{II} coordination polymers based on amino-functionalized tri-phenyl tetra-carboxylate: Bi-functional photo-luminescent sensing for Fe³⁺ and antibiotics. *Dyes Pigm.* **2019**, *170*, 107631.
- (16) Wang, Z. J.; Han, L. J.; Gao, X. J.; Zheng, H. G. Three Cd(II) MOFs with Different Functional Groups: Selective CO₂ Capture and Metal Ions Detection. *Inorg. Chem.* **2018**, *57*, 5232–5239.
- (17) Huang, W. H.; Ren, J.; Yang, Y. H.; Li, X. M.; Wang, Q.; Jiang, N.; Yu, J. Q.; Wang, F.; Zhang, J. Water-Stable Metal-Organic Frameworks with Selective Sensing on Fe³⁺ and Nitroaromatic Explosives, and Stimuli-Responsive Luminescence on Lanthanide Encapsulation. *Inorg. Chem.* **2019**, *58*, 1481–1491.
- (18) Ma, D.; Li, B.; Zhou, X.; Zhou, Q.; Liu, K.; Zeng, G.; Li, G.; Shi, Z.; Feng, S. A dual functional MOF as a luminescent sensor for quantitatively detecting the concentration of nitrobenzene and temperature. *Chem. Commun.* **2013**, *49*, 8964–8966.
- (19) He, H.; Zhu, Q.-Q.; Guo, M.-T.; Zhou, Q.-S.; Chen, J.; Li, C.-P.; Du, M. Doubly Interpenetrated Zn₄O-Based Metal-Organic Framework for CO₂ Chemical Transformation and Antibiotic Sensing. *Cryst. Growth Des.* **2019**, *19*, 5228–5236.
- (20) Kumar, G.; Pachisia, S.; Kumar, P.; Kumar, V.; Gupta, R. Zn- and Cd-based Coordination Polymers Offering H-Bonding Cavities: Highly Selective Sensing of S₂O₇²⁻ and Fe³⁺ Ions. *Chem. - Asian J.* **2019**, *14*, 4594–4600.
- (21) Yu, Y. e.; Wang, Y.; Xu, H.; Lu, J.; Wang, H.; Li, D.; Dou, J.; Li, Y.; Wang, S. Dual-responsive luminescent sensors based on two Cd-MOFs: rare enhancement toward acac and quenching toward Cr₂O₇²⁻. *CrystEngComm* **2020**, *22*, 3759–3767.
- (22) Bigdeli, F.; Lollar, C. T.; Morsali, A.; Zhou, H. C. Switching in Metal-Organic Frameworks. *Angew. Chem., Int. Ed.* **2020**, *59*, 4652–4669.
- (23) Tian, X. M.; Yao, S. L.; Qiu, C. Q.; Zheng, T. F.; Chen, Y. Q.; Huang, H.; Chen, J. L.; Liu, S. J.; Wen, H. R. Turn-On Luminescent Sensor toward Fe³⁺, Cr³⁺, and Al³⁺ Based on a Co(II) Metal-Organic Framework with Open Functional Sites. *Inorg. Chem.* **2020**, *59*, 2803–2810.
- (24) Yu, C.; Sun, X.; Zou, L.; Li, G.; Zhang, L.; Liu, Y. A Pillar-Layered Zn-LMOF with Uncoordinated Carboxylic Acid Sites: High Performance for Luminescence Sensing Fe³⁺ and TNP. *Inorg. Chem.* **2019**, *58*, 4026–4032.
- (25) Ding, M.; Cai, X.; Jiang, H.-L. Improving MOF stability: approaches and applications. *Chem. Sci.* **2019**, *10*, 10209–10230.
- (26) Singha, D. K.; Majee, P.; Hui, S.; Mondal, S. K.; Mahata, P. Luminescent metal-organic framework-based phosphor for the detection of toxic oxoanions in an aqueous medium. *Dalton Trans.* **2020**, *49*, 829–840.
- (27) Das, R.; Dhankhar, S. S.; Nagaraja, C. M. Construction of a bifunctional Zn(II)-organic framework containing a basic amine functionality for selective capture and room temperature fixation of CO₂. *Inorg. Chem. Front.* **2020**, *7*, 72–81.
- (28) ZareKarizi, F.; Joharian, M.; Morsali, A. Pillar-layered MOFs: functionality, interpenetration, flexibility and applications. *J. Mater. Chem. A* **2018**, *6*, 19288–19329.
- (29) Stolar, T.; Užarević, K. Mechanochemistry: an efficient and versatile toolbox for synthesis, transformation, and functionalization of porous metal-organic frameworks. *CrystEngComm* **2020**, *22*, 4511–4525.
- (30) Feng, Y.; Wang, Z.; Fan, W.; Kang, Z.; Feng, S.; Fan, L.; Hu, S.; Sun, D. Engineering the pore environment of metal-organic framework membranes via modification of the secondary building unit for improved gas separation. *J. Mater. Chem. A* **2020**, *8*, 13132–13141.
- (31) Zhang, F.; Yao, H.; Zhao, Y.; Li, X.; Zhang, G.; Yang, Y. Mixed matrix membranes incorporated with Ln-MOF for selective and sensitive detection of nitrofurans antibiotics based on inner filter effect. *Talanta* **2017**, *174*, 660–666.
- (32) Zhang, X.; Zhang, Q.; Yue, D.; Zhang, J.; Wang, J.; Li, B.; Yang, Y.; Cui, Y.; Qian, G. Flexible Metal-Organic Framework-Based Mixed-Matrix Membranes: A New Platform for H₂S Sensors. *Small* **2018**, *14*, 1801563.
- (33) Zhu, Q. Q.; He, H.; Yan, Y.; Yuan, J.; Lu, D. Q.; Zhang, D. Y.; Sun, F.; Zhu, G. An Exceptionally Stable Tb(III)-Based Metal-Organic Framework for Selectively and Sensitive Detecting Antibiotics in Aqueous Solution. *Inorg. Chem.* **2019**, *58*, 7746–7753.
- (34) Lu, Y. Z. H.; Zhang, H. C.; Chan, J. Y.; Ou, R. W.; Zhu, H. J.; Forsyth, M.; Marjanovic, E. M.; Doherty, C. M.; Marriott, P. J.; Holl, M. M. B.; Wang, H. T. Homochiral MOF-Polymer Mixed Matrix Membranes for Efficient Separation of Chiral Molecules. *Angew. Chem., Int. Ed.* **2019**, *58*, 16928–16935.
- (35) Howlader, P.; Mukherjee, P. S. Solvent Directed Synthesis of Molecular Cage and Metal Organic Framework of Copper(II) Paddlewheel Cluster. *Isr. J. Chem.* **2019**, *59*, 292–298.
- (36) Bhattacharyya, S.; Maity, M.; Chowdhury, A.; Saha, M. L.; Panja, S. K.; Stang, P. J.; Mukherjee, P. S. Coordination-Assisted Reversible Photoswitching of Spiropyran-Based Platinum Macrocycles. *Inorg. Chem.* **2020**, *59*, 2083–2091.
- (37) Huang, C.; Zhu, K.; Zhang, Y.; Lu, G.; Shao, Z.; Gao, K.; Mi, L.; Hou, H. Surfactant-assisted assembly of nanoscale zinc coordination compounds to enhance tandem conversion reactions in water. *Dalton Trans.* **2019**, *48*, 16008–16016.
- (38) Pan, X.; Wang, X.; Wang, X.; Li, Y.; Liu, G.; Lin, H. Various types of isopolymolybdate-based metal-organic complexes formed in different conditions: synthesis, structures, luminescence, electrochemical, and photocatalytic performances. *CrystEngComm* **2019**, *21*, 6472–6481.
- (39) Lin, L. D.; Li, Z.; Liu, J. H.; Sun, Y. Q.; Li, X. X.; Zheng, S. T. A new type of composite MOFs based on high-valent Sb(V)-based units and cuprous-halide clusters. *Chem. Commun.* **2019**, *55*, 15113–15116.
- (40) Gutierrez-Tarrino, S.; Olloqui-Sariego, J. L.; Calvente, J. J.; Palomino, M.; Minguez Espallargas, G.; Jorda, J. L.; Rey, F.; Ona-Burgos, P. Cobalt Metal-Organic Framework Based on Two Dinuclear Secondary Building Units for Electrocatalytic Oxygen Evolution. *ACS Appl. Mater. Interfaces* **2019**, *11*, 46658–46665.
- (41) Catarineu, N. R.; Schoedel, A.; Urban, P.; Morla, M. B.; Trickett, C. A.; Yaghi, O. M. Two Principles of Reticular Chemistry Uncovered in a Metal-Organic Framework of Heterotritopic Linkers and Infinite Secondary Building Units. *J. Am. Chem. Soc.* **2016**, *138*, 10826–10829.
- (42) Sharma, M. K.; Senkovska, I.; Kaskel, S.; Bharadwaj, P. K. Three-dimensional porous Cd(II) coordination polymer with large one-dimensional hexagonal channels: high pressure CH₄ and H₂ adsorption studies. *Inorg. Chem.* **2011**, *50*, 539–544.
- (43) Sheldrick, G. M. A short history of SHELX. *Acta Crystallogr., Sect. A: Found. Crystallogr.* **2008**, *64*, 112–122.
- (44) Pei, W. Y.; Yang, J.; Wu, H.; Zhou, W.; Yang, Y. W.; Ma, J. F. A calix[4]resorcinarene-based giant coordination cage: controlled assembly and iodine uptake. *Chem. Commun.* **2020**, *56*, 2491–2494.
- (45) Ngue, C. M.; Leung, M. K.; Lu, K. L. An Electroactive Zinc-based Metal-Organic Framework: Bifunctional Fluorescent Quenching Behavior and Direct Observation of Nitrobenzene. *Inorg. Chem.* **2020**, *59*, 2997–3003.
- (46) Blatov, V. A.; Shevchenko, A. P.; Proserpio, D. M. Applied Topological Analysis of Crystal Structures with the Program Package ToposPro. *Cryst. Growth Des.* **2014**, *14*, 3576–3586.
- (47) Spek, A. L. Single-Crystal Structure Validation with the Program PLATON. *J. Appl. Crystallogr.* **2003**, *36*, 7–13.
- (48) Dhaka, S.; Kumar, R.; Deep, A.; Kurade, M. B.; Ji, S.-W.; Jeon, B.-H. Metal-organic frameworks (MOFs) for the removal of emerging

contaminants from aquatic environments. *Coord. Chem. Rev.* **2019**, *380*, 330–352.

(49) Li, N.; Xu, J.; Feng, R.; Hu, T. L.; Bu, X. H. Governing metal-organic frameworks towards high stability. *Chem. Commun.* **2016**, *52*, 8501–8513.

(50) Singh Dhankhar, S.; Sharma, N.; Kumar, S.; Dhilip Kumar, T. J.; Nagaraja, C. M. Rational Design of a Bifunctional, Two-Fold Interpenetrated Zn(II)-Metal-Organic Framework for Selective Adsorption of CO₂ and Efficient Aqueous Phase Sensing of 2,4,6-Trinitrophenol. *Chem. - Eur. J.* **2017**, *23*, 16204–16212.

(51) Chand, S.; Pal, A.; Das, M. C. A Moisture-Stable 3D Microporous Co^{II}-Metal-Organic Framework with Potential for Highly Selective CO₂ Separation under Ambient Conditions. *Chem. - Eur. J.* **2018**, *24*, 5982–5986.

(52) Pal, A.; Chand, S.; Madden, D. G.; Franz, D.; Ritter, L.; Space, B.; Curtin, T.; Chand Pal, S.; Das, M. C. Immobilization of a Polar Sulfone Moiety onto the Pore Surface of a Humid-Stable MOF for Highly Efficient CO₂ Separation under Dry and Wet Environments through Direct CO₂-Sulfone Interactions. *ACS Appl. Mater. Interfaces* **2020**, *12*, 41177–41184.

(53) Schlapbach, L.; Züttel, A. Hydrogen-storage materials for mobile applications. *Nature* **2001**, *414*, 353–358.

(54) Rowsell, J. L. C.; Millward, A. R.; Park, K. S.; Yaghi, O. M. Hydrogen Sorption in Functionalized Metal-Organic Frameworks. *J. Am. Chem. Soc.* **2004**, *126*, 5666–5667.

(55) Das, P.; Mandal, S. K. Strategic Design and Functionalization of an Amine-Decorated Luminescent Metal Organic Framework for Selective Gas/Vapor Sorption and Nanomolar Sensing of 2,4,6-Trinitrophenol in Water. *ACS Appl. Mater. Interfaces* **2018**, *10*, 25360–25371.

(56) Kang, X.-M.; Fan, X.-Y.; Hao, P.-Y.; Wang, W.-M.; Zhao, B. A stable zinc-organic framework with luminescence detection of acetylacetone in aqueous solution. *Inorg. Chem. Front.* **2019**, *6*, 271–277.

(57) Khatua, S.; Biswas, P. Flexible Luminescent MOF: Trapping of Less Stable Conformation of Rotational Isomers, In Situ Guest-Responsive Turn-Off and Turn-On Luminescence and Mechanistic Study. *ACS Appl. Mater. Interfaces* **2020**, *12*, 22335–22346.

(58) Huang, Y. W.; Chuang, P. M.; Wu, J. Y. Solvent-Induced Controllable Supramolecular Isomerism: Phase Transformation, CO₂ Adsorption, and Fluorescence Sensing toward CrO₄²⁻, Cr₂O₇²⁻, MnO₄⁻, and Fe³⁺. *Inorg. Chem.* **2020**, *59*, 9095–9107.

(59) Liu, L.; Wang, Y.; Lin, R.; Yao, Z.; Lin, Q.; Wang, L.; Zhang, Z.; Xiang, S. Two water-stable lanthanide metal-organic frameworks with oxygen-rich channels for fluorescence sensing of Fe(III) ions in aqueous solution. *Dalton Trans.* **2018**, *47*, 16190–16196.

(60) Liu, C. H.; Guan, Q. L.; Yang, X. D.; Bai, F. Y.; Sun, L. X.; Xing, Y. H. Polyiodine-Modified 1,3,5-Benzenetricarboxylic Acid Framework Zn(II)/Cd(II) Complexes as Highly Selective Fluorescence Sensors for Thiamine Hydrochloride, NACs, and Fe³⁺/Zn²⁺. *Inorg. Chem.* **2020**, *59*, 8081–8098.

(61) Singh, M.; Senthilkumar, S.; Rajput, S.; Neogi, S. Pore-Functionalized and Hydrolytically Robust Cd(II)-Metal-Organic Framework for Highly Selective, Multicyclic CO₂ Adsorption and Fast-Responsive Luminescent Monitoring of Fe(III) and Cr(VI) Ions with Notable Sensitivity and Reusability. *Inorg. Chem.* **2020**, *59*, 3012–3025.

(62) Yu, Y.; Wang, Y.; Yan, H.; Lu, J.; Liu, H.; Li, Y.; Wang, S.; Li, D.; Dou, J.; Yang, L.; Zhou, Z. Multiresponsive Luminescent Sensitivities of a 3D Cd-CP with Visual Turn-on and Ratiometric Sensing toward Al³⁺ and Cr³⁺ as Well as Turn-off Sensing toward Fe³⁺. *Inorg. Chem.* **2020**, *59*, 3828–3837.

(63) Shi, Y.-S.; Liu, D.; Fu, L.; Li, Y.-H.; Dong, G.-Y. Five water-stable luminescent Cd^{II}-based metal-organic frameworks as sensors for highly sensitive and selective detection of acetylacetone, Fe³⁺ and Cr₂O₇²⁻ ions. *CrystEngComm* **2020**, *22*, 4079–4093.

(64) Yu, H.-H.; Chi, J.-Q.; Su, Z.-M.; Li, X.; Sun, J.; Zhou, C.; Hu, X.-L.; Liu, Q. A water-stable terbium metal-organic framework with functionalized ligands for the detection of Fe³⁺ and Cr₂O₇²⁻ ions in

water and picric acid in seawater. *CrystEngComm* **2020**, *22*, 3638–3643.

(65) Qin, B.-W.; Zhang, X.-Y.; Zhang, J.-P. A stable multifunctional cadmium-organic framework based on 2D stacked layers: Effective gas adsorption, and excellent detection of Cr³⁺, CrO₄²⁻, and Cr₂O₇²⁻. *Dyes Pigm.* **2020**, *174*, 108011.

(66) Zhang, Y.-Q.; Blatov, V. A.; Lv, X.-X.; Yang, C.-H.; Qian, L.-L.; Li, K.; Li, B.-L.; Wu, B. Construction of five zinc coordination polymers with 4-substituted bis(triazole) and multicarboxylate ligands: Syntheses, structures and properties. *Polyhedron* **2018**, *155*, 223–231.

(67) Wang, C.-X.; Xia, Y.-P.; Yao, Z.-Q.; Xu, J.; Chang, Z.; Bu, X.-H. Two luminescent coordination polymers as highly selective and sensitive chemosensors for Cr^{VI}-anions in aqueous medium. *Dalton Trans.* **2019**, *48*, 387–394.

(68) Li, B.; Yan, Q.-Q.; Yong, G.-P. A new porous coordination polymer reveals selective sensing of Fe³⁺, Cr₂O₇²⁻, CrO₄²⁻, MnO₄⁻ and nitrobenzene, and stimuli-responsive luminescence color conversions. *J. Mater. Chem. C* **2020**, *8*, 11786–11795.

(69) Xu, H.; Zhai, B.; Cao, C. S.; Zhao, B. A Bifunctional Europium-Organic Framework with Chemical Fixation of CO₂ and Luminescent Detection of Al³⁺. *Inorg. Chem.* **2016**, *55*, 9671–9676.

(70) Zhang, C.; Shi, H.; Sun, L.; Yan, Y.; Wang, B.; Liang, Z.; Wang, L.; Li, J. Water Stable Metal-Organic Framework Based on Phosphono-containing Ligand as Highly Sensitive Luminescent Sensor toward Metal Ions. *Cryst. Growth Des.* **2018**, *18*, 7683–7689.

(71) Huang, J.-J.; Yu, J.-H.; Bai, F.-Q.; Xu, J.-Q. White-Light-Emitting Materials and Highly Sensitive Detection of Fe³⁺ and Polychlorinated Benzenes Based on Ln-Metal-Organic Frameworks. *Cryst. Growth Des.* **2018**, *18*, 5353–5364.

(72) Zhao, J.; Wang, Y. N.; Dong, W. W.; Wu, Y. P.; Li, D. S.; Zhang, Q. C. A Robust Luminescent Tb(III)-MOF with Lewis Basic Pyridyl Sites for the Highly Sensitive Detection of Metal Ions and Small Molecules. *Inorg. Chem.* **2016**, *55*, 3265–3271.